A modulation model for mode splitting of magnetic perturbations in the Mega Ampere Spherical Tokamak

M. J. Hole †§ and L. C. Appel

Euratom/UKAEA Fusion Association, Culham Science Centre, Abingdon, Oxon OX14 3DB, UK

† Research School of Physical Sciences and Engineering, Australian National University, ACT 0200, Australia

Abstract.

Recent observations of magnetic fluctuation activity in the Mega Ampere Spherical Tokamak (MAST) reveal the presence of plasmas with bands of both low and high frequency magnetic fluctuations. Such plasmas exhibit a spectrum of low frequency modes with adjacent toroidal mode numbers, for which the measured frequency is near the Doppler shifted rotation frequency of the plasma. These are thought to be tearing modes. Also present are a spectrum of high frequency modes (*e.g.* Alfvén, fishbone and/or ICE). The frequency and mode number of the tearing mode and its harmonics is identical to the frequency and mode number splitting of the high frequency MHD activity, strongly suggesting that the high frequency splitting is produced by modulation of the high and low frequency modes. We describe a strong modulation model, in which the nonlinear terms are fitted to produce the amplitude envelope profile of the tearing mode. A bispectral analysis proves that the low frequency modes are indeed in phase with the fundamental, while Fourier-SVD mode analysis confirms the mode numbers are toroidal harmonics. Employing this model, the side-band amplitude profile of the high frequency modes is predicted, and found to be in good agreement with experimental observations. Also, toroidal mode number splitting of the high frequency activity matches the mode number of the tearing mode. Weak evidence is found to indicate the Alfvénic sidebands are in phase with the Alfvén eigenmode fundamental. The findings support predictions of a strong modulation model, and suggest a need to further develop nonlinear MHD theory to predict the amplitude of coupled sidebands, and so corroborate the observed nonlinear plasma response.

PACS numbers: 52.35.Bj, 52.35.Mw, 52.55.Fa, 52.70.Ds

§ To whom correspondence should be addressed (matthew.hole@anu.edu.au)

1. Introduction

Fine scale frequency splitting of Alfvénic modes has received much attention in recent years. Fasoli [1] was the first to report fine splitting of fast particle driven toroidal Alfvén eigenmodes (TAE's) in tokamaks. In these neutral beam and ICRH heated plasmas, different bands of $n = 5$ to 12 mode numbers in the frequency range 200-500 kHz were observed. These were identified as toroidal Alfvén eigenmodes, with frequency spacing of 25 kHz for different n modes and which was shown to be consistent with the Doppler shift from the plasma rotation. Within each band, a second level of fine scale frequency splitting was also observed, with $\Delta f \approx 2$ kHz. In other work, Fasoli *et al* [2] postulated that this fine scale splitting may be explained by a nonlinear model of near threshold regimes for kinetic instabilities [3]. When the linear growth rate of each TAE exceeds a certain value, period doubling bifurcations occur which split the original spectral line into a number of sidebands with equidistant frequency spacing and the same toroidal mode number. These predicted sidebands have frequency that compares well to the observed spacing.

In more recent work, frequency splitting of MHD modes on different scales has been observed when driving Compressional Alfvén Eigenmodes (CAEs). In NSTX plasmas, Gorelenkov *et al* [4, 5] observe frequency splitting on three scales, which they propose corresponds to modes with adjacent toroidal, poloidal and radial mode number spacings with frequency splitting $\Delta f_n, \Delta f_m$, and Δf_s respectively, and with $\Delta f_n < \Delta f_m < \Delta f_s$. Numerical predictions of frequency splitting, using weak [6] and strong [7, 8] toroidicity theory yield: $\Delta f_n = 25$ kHz, $\Delta f_m = 218$ kHz, $\Delta f_s = 436$ kHz, and $\Delta f_n = 200-250$ kHz, $\Delta f_m = 150-250$ kHz,$\Delta f_s = 500-780$ kHz respectively, compared to observed values of $\Delta f_n = 20$ kHz, $\Delta f_m = 120$ kHz, $\Delta f_s = 1000$ kHz. Weak toroidicity theory assumes the poloidal mode number m and aspect ratio are large, and the oscillation frequency is in the range $\omega_{ci} \ll \omega < \omega_{ce}$, with ω_{ci} and ω_{ce} the ion and electron frequency, respectively.[6] In contrast, strong toroidicity theory [7, 8] assumes low aspect ratio, and solves for the eigenmode using a variational method assuming a ballooning expansion for the poloidal dependence of the eigenfunction. Different strong toroidicity formulations vary in their formulation of the Lagrangian and in their treatment of the Hall effect: these account for the frequency band ranges given for strong toroidicity theory. For all the models considered however, agreement between the predicted and observed frequency gaps is not quantitatively exact, especially for toroidal spacing in the strong toroidicity model. Gorelenkov *et al* [5] suggest a possible resolution is in the inclusion of ω/ω_c effects in the Hall term of the strong toroidicity model, as well as the retention of finite Larmor radius effects. In other work, similarity experiments on DIII-D [9] reveal fine splitting of CAE's at three different frequency spacings: 20kHz, 110kHz and 800kHz. These spacings do not change with the Alfvén velocity v_A inferred from interferometer measurements using a static equilibrium, and do not agree with either the analytical formulation of Gorelenkov *et al* [4] or more recent work by Smith *et al* [8]. Heidbrink *et al* [9] propose that the discrepancy may be resolved by the use of more accurate equilibria, the inclusion of

toroidal rotation, or that the splitting has it's origin in nonlinear effects. Finally, in all published work on CAEs which feature frequency splitting with different toroidal mode numbers, the main corroborating evidence is the measured toroidal mode number. In this paper we also undertake a bispectral analysis of the observed coherent modes.

Recently, Appel *et al* [10] have shown evidence of frequency splitting of CAEs in MAST. The frequency splitting occurs at two levels, $f = 20$ kHz and $f = 120$ kHz. Both bands have the same toroidal mode number spacing ($n = 1$), and the frequency evolution of each band is consistent with the Alfvén scaling, computed using an evolving equilibrium. Also present in these plasmas were low frequency modes, with near identical frequency spacing. Using the strong toroidicity theory of Smith *et al* [8], Appel *et al* found good agreement between the predicted and observed larger scale frequency spacing and mode numbers. At the finer scale, Appel *et al* proposed that the frequency splitting arises due to modulation between large amplitude low frequency and a single high frequency mode. Physically, the low frequency modes are long-lived, coherent and near stationary in the plasma frame, with $n \neq 0$. As such, they can be thought of as either a weak 3D equilibrium structure, or equivalently large amplitude perturbations interacting non-linearly in a 2D field configuration.

Given the possibility of large amplitude Alfvén eigenmodes causing fast particle loss, understanding the origin of fine splitting may have important consequences for confinement. Except for the case of ultra-fine splitting of Fasoli *et al* [2], for which the mode numbers were all the same, previous work has appealed to quantization of the dispersion relation, and the drive of separate linear modes, to explain fine scale splitting. In this work, we build on Appel *et al* and develop a modulation model between high and low frequency modes to describe high frequency splitting. The modulation model is not unique to a particular type of wave oscillation. We offer a simple phenomenological model to describe the modulation as a nonlinear interaction, and test it against examples of CAE activity in MAST. The model offers an alternate explanation in some cases for the observed frequency splitting.

To prove the modulation model is consistent with the data we compare the amplitude profile and mode numbers of predicted and observed spectral components, thereby establishing amplitude and mode coupling, and we use the bispectrum, a higher order spectral technique [11, 12], to demonstrate frequency and phase coupling. The combination of these attributes is very strong evidence of nonlinear interaction. Finally, borrowing from the space and astrophysical literature, we suggest a tractable approach to yield complementary nonlinear MHD theory predictions that would corroborate the observed nonlinear plasma response.

The paper is structured as follows: Sec. 2 presents some examples of modulation of magnetic activity in MAST, offering motivation for a modulation description. Section 3 introduces a nonlinear modulation model as well as the bispectrum. Section 4 performs a detailed study of specific magnetic activity in MAST, and fits the observed data to the model, yielding weighting coefficients. Finally, Sec. 5 discusses the significance of the nonlinear fit, and offers some suggestions for future theoretical work that might

elucidate the nonlinear interaction.

2. Evidence for modulation of magnetic activity in MAST

Evidence of modulation of high frequency data is now common in MAST. We present three examples: #15770, which exhibits $n = 2$ fishbone activity modulated by an $n = 3$ mode, and #17953 and #9429, both of which exhibit CAE activity with modulation by a strong low frequency $n = 1$ mode. One of these is then selected for further analysis. All examples are provided by spectra of signals of δB_ϕ, as measured from an outboard Outboard Mirnov Array for High-frequency Acquisition (OMAHA) [13, 14] coil. The computed Fourier amplitude $\delta B_\phi(\omega)$ is related to the coil voltage via

$$\delta B(\omega) = \frac{H(\omega)V_m(\omega)}{i\omega NA} \tag{1}$$

Here, $H(\omega)$ is the system transfer function, which is approximately unity in the MAST OMAHA system.

Figure 1 is a spectrum of δB_ϕ computed for discharge #15770, which was a low beam power heated $P_{NBI} = 0.6$ MW plasma with high plasma current $I_p = 1050$ kA taken during an Alfvén cascade MHD campaign. A constant frequency $n = 3$ mode can be identified at 30kHz, where the eigenmode number has been identified by Fourier-SVD [15] reconstruction. Also present is an $n = 2$ fishbone with frequency chirping down from 95kHz at 190ms. At a frequency of $95 - 30 = 60$ kHz is a $n = -1$ fishbone, consistent in mode number and frequency with modulation of the $n = 2$ and $n = 3$ modes.

Figure 2 shows evidence of magnetic fluctuation activity in high performance discharge #17953, which featured 3.1 MW of beam power and a plasma current peaking at $I_p = 950$ kA. Two bands of coherent magnetic fluctuations are present around 1.25MHz and 1.45MHz which we postulate are CAE's. The lower band has a frequency spacing of 8kHz with the peak amplitudes of each sub-band fluctuation forming an envelope around 1.262MHz. The upper band exhibits a similar frequency spacing but the amplitude variation appears to be more complicated in this case. During the observed high frequency activity there is also a 8kHz mode present.

Finally, Fig. 3 shows evidence of bands of high frequency (200-500 kHz) and low frequency (0-60 kHz) magnetic activity in discharge #9429. Both high and low frequency bands exhibit fine frequency structure, and the frequency spacing between low and high frequency modes is identical, at 16kHz. The presence of both low and high frequency modes in the same data set, as well as the sideband richness, motivates our selection of #9429 for more detailed analysis.

Discharge #9429 was a deuterium plasma with 1.25MW, 45keV deuterium NBI applied during the current ramp from 100-350ms, and 600kW ECRH applied from 210-290ms. The plasma current plateaus at 780kA, and is in H-mode from 158ms. Up to 200ms there is intermittent bursting high frequency activity. Two upward chirping bands separated by 150 kHz can be identified. Each band consists of a dominant mode ($n = 8$ and $n = 9$ for upper and lower band respectively), and sideband modes of smaller

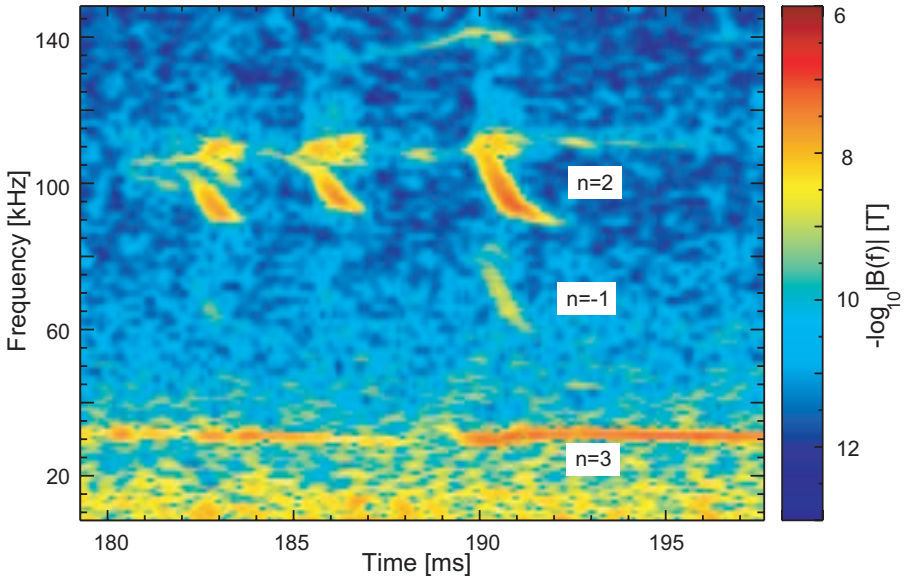

Figure 1. Spectrum of #15770. The $n = -1$ feature at 190ms is consistent with modulation of the $n = 3$ frequency-stationary and $n = 2$ frequency chirping fishbone.

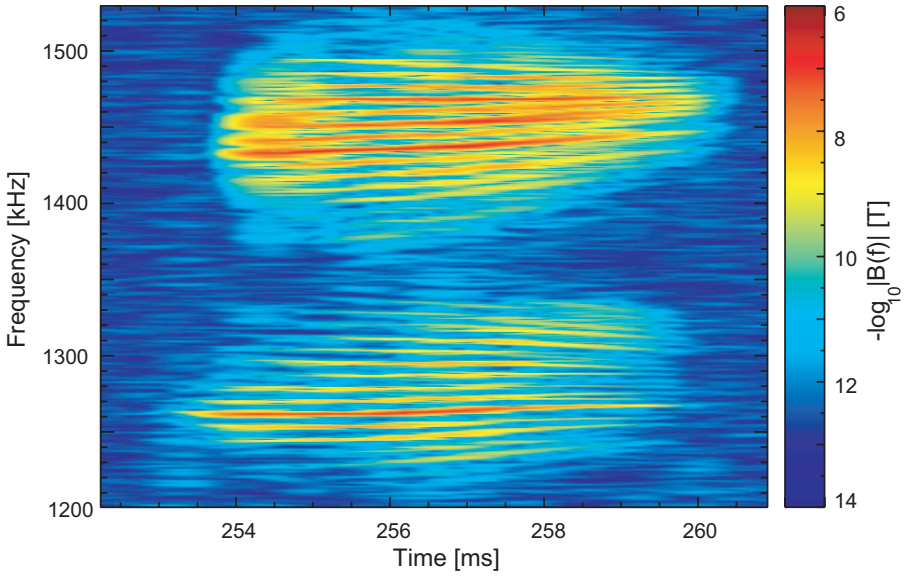

Figure 2. Spectrum of #17953, showing evidence of CAE activity in two bands at 1.25 MHz and 1.45 MHz around 254 ms. The frequency splitting is 8 kHz.

amplitude with 16 kHz spacing. A separate mode analysis [15] reveals the mode number spacing of these weaker sidebands is $\Delta n = 1$. A detailed physics analysis [10] suggests that these are CAE's, aliased in frequency from 1.4 to 1.9 MHz.

Also present are low frequency modes (≈ 16 kHz) and their harmonics, with toroidal mode numbers $n = 1, 2, 3, 4, 5$. Figure 4 shows the detailed evolution of #9429 in the latter phase of the discharge. The fundamental has features consistent with $m/n = 2/1$ tearing modes in other MAST discharges [16, 17]. For instance, the EFIT inferred on-axis safety factor q_0 is less than two throughout the discharge, and in the range

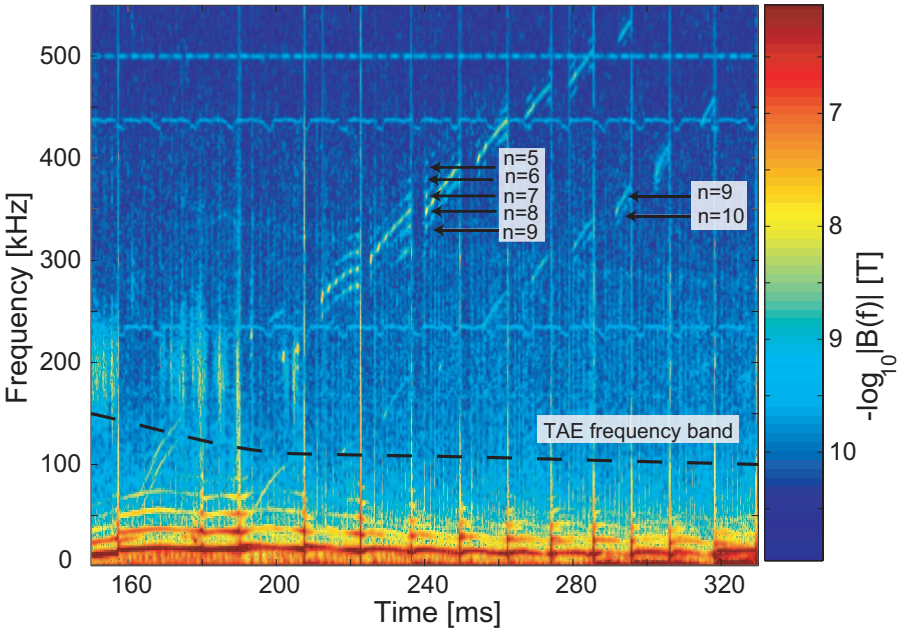

Figure 3. Spectrum of #9429, showing evidence of both CAE and tearing mode activity. The frequency splitting at low and high frequency match.

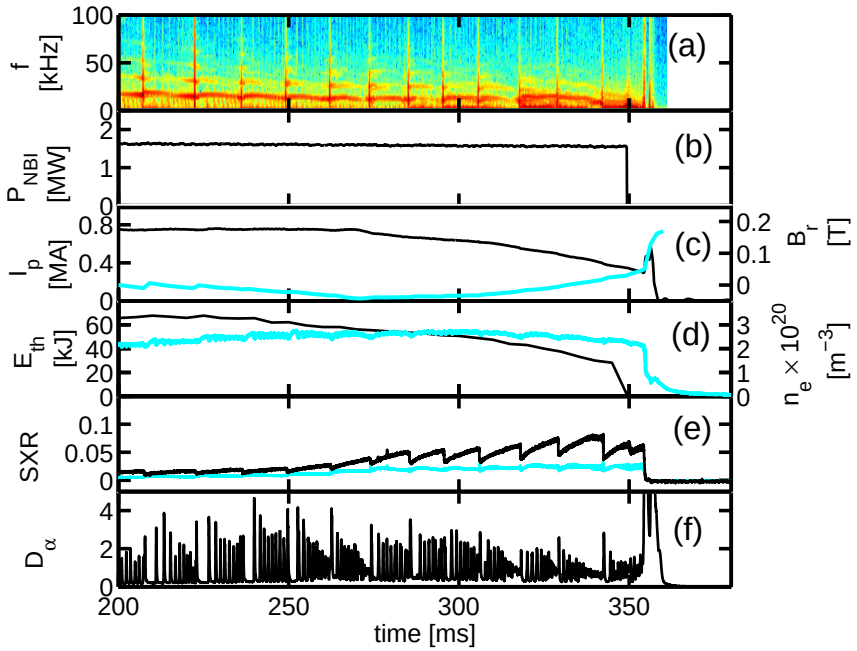

Figure 4. Evolution of #9429 prior to disruption. Figure (a) is a spectrogram of an outboard OMAHA δB_Z coil, while figure (b) shows the neutral beam heating power, (c) shows the plasma current I_p (heavy, left axis) and radial field B_r computed by integrating an outboard radial field coil signal (light, right axis), (d) shows the stored energy E_{th} computed from EFIT (heavy, left axis) and line averaged electron density n_e (light, right-axis), (e) shows emissivity of the core (heavy, left-axis) and half of the off-axis (light, right-axis) chord integrated soft x-ray traces, and (g) shows the light emission intensity from D_α at the plasma edge.

$1 < q_0 < 2$ from 110ms to 275ms, consistent with excitation of a $m/n = 2/1$ mode. From $\approx$ 162 ms, sawteeth are first observed in the soft x-ray emission, and coincide with entry of the plasma into H-mode [10]. Despite this, and comparing panel (a) and (e) of Fig. 4, the amplitude of the mode is largely unaffected by sawtooth crashes, distinguishing it from core MHD associated with sawteeth. As the mode frequency reduces, the radial field component B_r, computed by integrating the voltage from an outboard radial Mirnov coil from the OMAHA array, grows. Mode locking occurs at 354 ms. At this time, sawteeth disappear, the plasma density and stored energy drop rapidly, and an increase in D^{α} emission occurs from the divertor. Disruption is complete by 360 ms, at which time the plasma current drops to zero.

Appel *et al* [10] postulate that the sidebands observed in each CAE band are the result of nonlinear modulation of a single CAE and low frequency mode. The primary motivation offered was the near identical frequency spacing observed between low and high frequency modes. We explore this hypothesis further, and propose that the observed spectrum of modes results from the nonlinear modulation of two wave structures, each with a single well defined toroidal mode number, mode amplitude and phase. The interaction of these structures then produces a spectrum of modes with determined mode numbers, amplitudes and phase. To verify this hypothesis, we next introduce both a mathematical model for the wave interaction, and a tool to compute the phase relationships between the different modes.

3. A nonlinear modulation model

Our modulation model comprises the superposition of linear Fourier signals driven nonlinearly. Specifically, we suppose the sum of M linear modes

$$x_p = \sum_{i=1}^{M} A_i \cos(\omega_i t + \Phi_i) \tag{2}$$

is driven nonlinearly to N'th order. That is,

$$y_N = \sum_{i=1}^{N} \beta_i x_p^i + x_{noise} \tag{3}$$

where y_N is the nonlinearly driven signal. Here, the i'th plasma mode has amplitude A_i, angular frequency ω_i and phase angle Φ_i. The nonlinear model comprises the sum of powers of x_p, with real coefficient β_i denoting the nonlinearity strength of the i'th power, together with a noise amplitude x_{noise}. In general, the signal of Eq. (2), when driven by the nonlinear model of Eq. (3) can always be written as the Fourier series

$$x_{p,NL} = \sum_{i=1}^{Q} \alpha_i(\beta_1, ..., \beta_N) \cos(\Omega_i t + \chi_i) + x_{noise} \tag{4}$$

where the subscript NL denotes nonlinear, and where α_i, Ω_i and χ_i are Fourier signal amplitude, angular frequency and angle, respectively. The number of terms in the

expansion is Q, and Ω_i is taken from the list of fundamental, harmonic, sum and difference frequencies.

Expressions for α_i, Ω_i and χ_i can be derived by multinomial expansion. Writing $x_p = \sum_{i=1}^{M} A_i/2\left[\exp(j(\omega_i t + \Phi_i)) + \exp(-j(\omega_i t + \Phi_i))\right]$ then Eq. (3) expands as

$$x_{p,NL} = \sum_{n=1}^{N}\sum_{k_1=0}^{n}\sum_{k_2=0}^{n-k_1}\cdots\sum_{k_{2M-1}=0}^{n-k_1-\ldots-k_{2M-2}}\prod_{i=1}^{M}\frac{\beta_n}{2^n}\begin{pmatrix} n \\ k_1, k_2, ..., k_{2M}\end{pmatrix}\times$$
$$A_i^{k_i+k_{M+i}}\exp\left[j(k_i-k_{M+i})\omega_i t + j(k_i-k_{M+i})\Phi_i\right] \;+\; x_{noise} \tag{5}$$

where $k_i \in \mathbb{N}$, k_i, k_{i+M} are the power indices of the ω_i and $-\omega_i$ components respectively, and $k_{2M} = n - k_1 - k_2 - ... - k_{2M-1}$. If the component frequencies belong to a linearly independent basis set, such that $(k_1 - k_{M+1})\omega_1 + (k_2 - k_{M+2})\omega_2 + ... + (k_M - k_{2M})\omega_M = 0$ holds only for $k_1 = k_2 = ... = k_{2M} = 0$, then each frequency peak corresponds to a unique combination of $k_1, k_2, ..., k_{2M}$ natural numbers. By comparing Eq. (4) to Eq. (5) the frequencies Ω_i, phase χ_i and amplitudes α_i in Eq. (4) can then be identified. An order n nonlinearly driven signal with frequency

$$\Omega_i = (k_1 - k_{M+1})\omega_1 + (k_2 - k_{M+2})\omega_2 + ... + (k_M - k_{2M})\omega_M \tag{6}$$

will hence have amplitude

$$\alpha_i(\beta_1, ..., \beta_N) = \frac{\beta_n}{2^n}\begin{pmatrix} n \\ k_1, k_2, ..., k_{2M}\end{pmatrix}\prod_{j=1}^{M} A_j^{k_j+k_{M+j}} \tag{7}$$

and phase

$$\chi_i = (k_1 - k_{M+1})\Phi_1 + (k_2 - k_{M+2})\Phi_2 + ... + (k_M - k_{2M})\Phi_M \tag{8}$$

For the case in which the nonlinearity is quadratic (*i.e.* $N = 2$), the signal is said to exhibit "quadratic phase coupling" [18]. For example, if the signal is the sum of two cosinusoids with frequencies ω_1 and ω_2 , $M = 2$, and y_{NL} comprises frequencies $\omega_1, \omega_2, 2\omega_1, 2\omega_2, \omega_1+\omega_2, \omega_1-\omega_2$ with corresponding phases $\Phi_1, \Phi_2, 2\Phi_1, 2\Phi_2, \Phi_1+\Phi_2, \Phi_1-\Phi_2$. More generally, a signal comprising two frequency components ω_1 and ω_2 with $\omega_2 > \omega_1$ driven to N'th order will comprise $2\sum_{k=1}^{N} k$ frequency components, whose sum is the arithmetic progression $2\sum_{k=1}^{N} k = N(N+1)$ [19], at angular frequencies $\omega_1, ..., N\omega_1, \omega_2-(N-1)\omega_1, ..., \omega_2+(N-1)\omega_1, 2\omega_2-(N-2)\omega_1, ..., 2\omega_2+(N-2)\omega_1, ..., (N-1)\omega_2-\omega_1, (N-1)\omega_2, (N-1)\omega_2+\omega_1, N\omega_2$.

For arbitrary N and $M = 1$ some special phase relationships result which warrant comment. If $\Phi_1 = 0$ the harmonics produced by the nonlinear model of a single mode will hence all be in phase, or if $\Phi_1 \neq 0$, have linear phase shift. The different phase relationships, in-phase, linear-phase shift and nonlinear-phase shift, can be understood by simple example. Figure 5 shows the Fourier reconstruction of a 20 kHz sawtooth, $x_s(t) = \sum_{k}^{N_k} \sin(2\pi f t + \Phi_k)/k$, with $N_k = 100$ harmonics. Also shown is a reconstruction of a Fourier series in which each harmonic has a linear phase shift $\Phi_k = k\Delta\Phi$ and nonlinear phase shift $\Phi_k = k^2\Delta\Phi$. Here, $\Delta\Phi \approx 0.94\pi$ is chosen for illustration, and all signals have the same power spectra. The sawtooth and the linearly-phase delayed

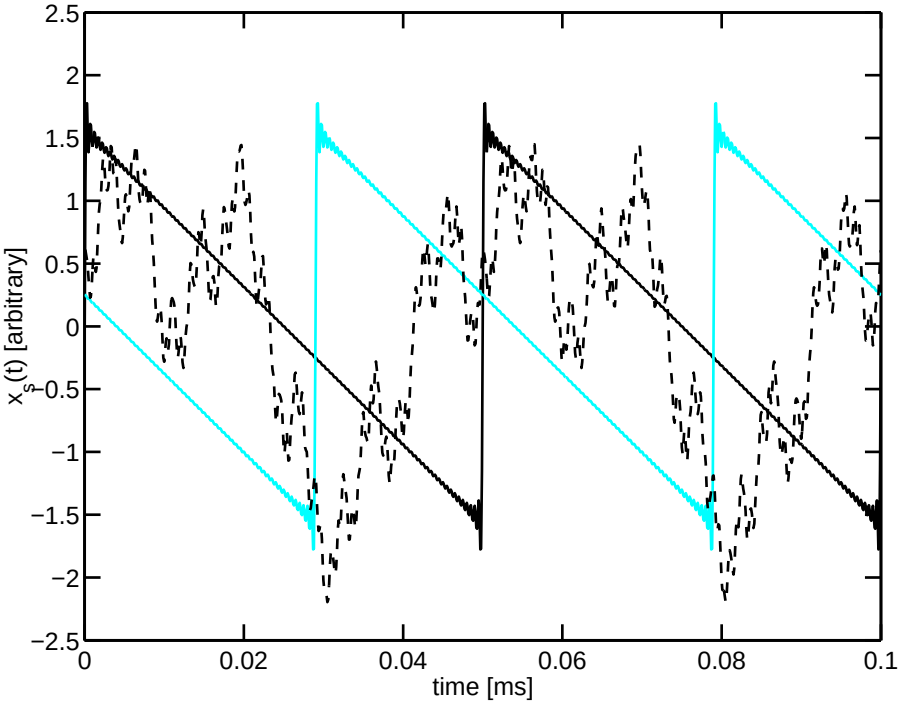

Figure 5. Reconstruction of a sawtooth waveform (heavy-line). All signals have identical power spectra, but differing Fourier transform, with linear (solid-line) and nonlinear (dashed-line) phase offsets.

sawtooth have identical temporal waveform with an overall temporal delay of $t' = \Phi_1/\omega$. Thus, linearly phase-shifted signals simply correspond to time-delayed signals. The temporal waveform of the nonlinearly phase shifted signal is however vastly different. Such signals, in which the phase shift is not a linear function of frequency, are said to exhibit phase distortion.

Higher order spectral tools, such as the bispectrum [11, 12], offer quantitative techniques to resolve and quantify the phase relationships between harmonics. The bispectrum is defined by

$$B(\omega_k, \omega_l) = \langle X(\omega_k) X(\omega_l) X^*(\omega_k + \omega_l) \rangle \tag{9}$$

where X is the Fourier transform of the signal computed over a time window Δt, and $*$ denotes the complex conjugate. The $\langle\rangle$ brackets denote an averaging operation over a time window $\Delta\tau$, with $\Delta\tau > \Delta t$. The bispectrum, with magnitude $|B|$ and biphase $\angle B$, identifies and resolves frequency components that satisfy the frequency coupling condition $\omega_k + \omega_l = \omega_{k+l}$. The properties of the bispectrum depend largely upon the phase $\angle X(\omega_k)X(\omega_l)X^*(\omega_k + \omega_l)$ over each window Δt. Three different types of signals produce different phase relationships[12]:

(i) For signals that are coherent over the interval $\Delta\tau$ and exhibit frequency coupling, but are not the result of nonlinear modulation, the phase $\angle X(\omega_k)X(\omega_l)X^*(\omega_k+\omega_l)$ will be the same for every window Δt within $\Delta\tau$. The biphase need not be zero.

That is, in general, $\Phi_l + \Phi_k - \Phi_{l+k} \neq 0$. Such a signal might correspond to three independently driven cavity modes with frequencies $\omega_1, \omega_2 = 2\omega_1$ and $\omega_3 = 3\omega_1$.

(ii) For signals that are the result of a quadratic nonlinearity the biphase at all peaks in the bispectrum amplitude (which correspond to signals with components at frequency ω_k, ω_l and $\omega_{k+l} = \omega_k + \omega_l$) is always zero. Extension to higher nonlinear order is a straight-forward generalisation. That is, if Ω^a, Ω^b and Ω^{a+b} are frequencies given by $\Omega^a = \sum_{i=1}^{M}(k_i^a - k_{M+i}^a)\omega_i$, $\Omega^b = \sum_{i=1}^{M}(k_i^b - k_{M+i}^b)\omega_i$, and $\Omega^{a+b} = \Omega^a + \Omega^b$, then using Eq. (8) we find

$$\angle B(\Omega^a, \Omega^b) = \sum_{i=1}^{M}\left[(k_i^a - k_{M+i}^a) + (k_i^b - k_{M+i}^b) - (k_i^a + k_i^b - k_{M+i}^a - k_{M+i}^b)\right]\Phi_i = 0 \quad (10)$$

Such signals satisfy the phase coupling condition $\Phi_l + \Phi_k = \Phi_{l+k}$. A plasma example is a single mode driven nonlinearly to large amplitude, producing harmonics.

(iii) For frequencies (ω_k, ω_l) which correspond to noise, the $\angle X(\omega_k)X(\omega_l)X^*(\omega_k + \omega_l)$ will be uniformly distributed. The averaging operation in the bispectrum has no effect on signals that are coherent, but serves to minimize the magnitude of the bispectrum value of noise, by sampling wave packets with different random biphase.

The presence of both frequency and phase coupling is very strong evidence that the signal comprises components that are the product of nonlinear modulation. The alternate possibility that the signal consists of independent cavity modes that exhibit frequency and phase coupling can still not be discounted, except through the principle of Occam's razor.

A measure of signal nonlinearity often used is the bicoherence [20]:

$$b^2(\omega_k, \omega_l) = \frac{|B(\omega_k, \omega_l)^2|}{\langle |X(\omega_k)X(\omega_l)|^2 \rangle \langle |X(\omega_k + \omega_l)|^2 \rangle} \quad (11)$$

which lies between zero and unity. A bicoherence of zero indicates no frequency coupling at frequencies ω_k, ω_l and $\omega_k + \omega_l$.. While a bicoherence of unity indicates frequency coupling, it does not necessarily imply phase coupling, especially if the signal is coherent over the window within which the averaging of Eq. (9) was performed. In this instance, to better distinguish between signals (i) and (ii), either the time window $\Delta\tau$ must be increased to span multiple wave bursts, or the biphase must be inspected. Increasing the time window is useful if multiple mutually-incoherent wave bursts exist, each of which exhibit a near identical power spectrum. In this case $|X(\omega_k)X(\omega_l)X^*(\omega_k + \omega_l)|$ will be similar at different bursts, but the angle $\angle X(\omega_k)X(\omega_l)X^*(\omega_k + \omega_l)$ will, in general, be different. The averaging in the bispectrum then becomes an ensemble average across different wave packets. Only signals that are phase-coupled will sum to produce a nonzero value of the bicoherence. Many plasma signals however are either coherent and long-lived, or if bursty, the frequency components evolve between wave-packets. In this case the bicoherence alone is insufficient to conclude phase-coupling, and inspection of the biphase is necessary.

Figure 6 shows an illustration of biphase averaging, showing uncoupled, coherent, and quadratic phase coupling examples. For a signal with no coupling between frequency

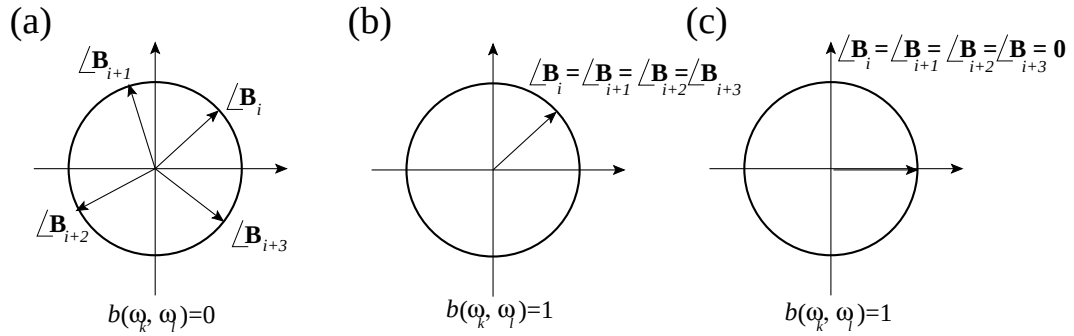

Figure 6. Illustration of the different types of signal couplings and respective realizations of the bispectrum, which ensemble average to form the bispectrum $B(\omega_k, \omega_l)$. Figure (a) is for uncoupled signals, figure (b) shows the coupling for coherent, but uncoupled signals, and (c) is for nonlinearly coupled signals. Also indicated is the corresponding bicoherence.

components, $\angle X(\omega_k)X(\omega_l)X^*(\omega_k + \omega_l)$ is random, and uniformly distributed over 2π. If the amplitude is also random and independent of angle, then $b = 0$. If the signal is coherent, then every realization of $X(\omega_k)X(\omega_l)X^*(\omega_k + \omega_l)$ will have the same phase, and $b = 1$. If the signal is driven nonlinearly however, then every realization of $X(\omega_k)X(\omega_l)X^*(\omega_k + \omega_l)$ will have zero phase, $b = 1$. When deriving conclusions from the bicoherence, it is hence important to check $\angle B$ if a nonlinear coupling conclusion is sought.

In recent years, higher order spectral techniques such as the bispectrum have found an increasing use in the study of mode coupling. Some examples in magnetic confinement include the study of the interaction of multiple neoclassical tearing modes (NTM's) [21], plasma turbulence [22], confinement transitions [23], and evidence of mode saturation in a laboratory plasma [24]. Raju *et al* [21] study the interaction of 3/2, 4/3 and 7/5 coupled modes in JET plasmas. By studying the time evolution of the bicoherence and mode amplitude, they were able to deduce that the 7/5 mode is driven by the 3/2 and 4/3 modes, and that the strong 4/3, 3/2 coupling may be responsible for the observed stabilization of the 4/3 mode on the 3/2 mode. Itoh *et al* [22] study the bicoherence of fluctuations in a test system comprising drift waves and zonal flows. They compute the response of a test mode to nonlinear interaction between a pair of modes in a turbulent plasma, and using this, compute the turbulent spectrum and bicoherence. Amongst other results, Itoh *et al* find the total bicoherence increases as the amplitude of the zonal flow increases. White *et al* [23] study the characteristics of the bicoherence calculated from D_α oscillations measured in the edge plasma of NSTX. Their main result is that the level of nonlinear coupling between between low and high frequency fluctuations does not vary in the 10ms prior to confinement transition. More recently, Austin *et al* [24], whose study of electrostatic fluctuations of a vacuum arc centrifuge [25] reveal the plasma is in a stochastic growth state [26], also employ the bicoherence to confirm the electrostatic modes are nonlinearly coupled.

A feature of the bispectrum is it's ability to remove noise, by ensemble averaging over different time windows. As discussed above, nearly all examples in the plasma literature focus on the application of the bicoherence. From a signal analysis perspective, an attractive feature of the bicoherence is it's normalization, giving an amplitude between zero and unity. Peaks in the bicoherence are evidence of frequency coupling. If the signals comprise an ensemble of mutually incoherent wave bursts, a peak in the bicoherence is also evidence of phase-coupling. The combination of frequency and phase coupling is very strong evidence that that the signal has a nonlinear origin. As discussed above however, for signals that are coherent over their entire duration, such as global ideal MHD modes, the study of the bicoherence alone is incomplete if trying to infer phase-coupling. The reason is that a peak will occur at $b(f_1, f_2)$ simply because the biphase of each realisation, given by $\Phi_l + \Phi_k - \Phi_{l+k}$ is the *same* for each realisation. In such cases the biphase must also be investigated to positively identify phase-coupling. In the next section we deploy bispectral analysis to investigate frequency and phase coupling relationships between harmonics and sidebands of coherent MAST magnetic perturbation data.

4. MHD activity in MAST

Figure 7 is a Fourier transform of magnetic activity at 220ms into #9429, computed over a 1ms time slice. This time is selected as both the low and high frequency components are well defined. We suppose a single $(m, n) = (1, 1)$ tearing mode is driven to fifth order in nonlinearity. Expanding Eq. (4) gives the α coefficients as a function of β. Next, the amplitudes of α are solved for the β coefficients, yielding: $\beta_1 = 1.0, \beta_2 = 0.34, \beta_3 = 6.0 \times 10^{-2}, \beta_4 = 6.4 \times 10^{-2}, \beta_5 = 5.7 \times 10^{-2}$.

Applying the nonlinear model to the superposition of a tearing mode at 16kHz (with mode amplitude 2 gauss), a CAE mode with frequency 280kHz (amplitude 31 mgauss) and Gaussian noise (with standard deviation 0.001V in the data), produces the fitted spectrum. For clarity in the predicted spectrum, the noise standard deviation has been chosen to be well below the standard deviation of the data. The frequency of all sidebands, together with the amplitudes of the CAE sidebands are predictions of the nonlinear model. Above the noise threshold, measured and predicted frequencies of the peaks in amplitude agree to within 5%, whilst the amplitudes of CAE sidebands are in agreement to within a factor of two. The former is strong evidence of frequency-coupling, and the latter evidence of amplitude-coupling.

The value of computing the bispectrum is in verifying frequency-coupling, and computing phase relationships. Figure 8(a) and 8(b) are plots of the simulated and measured bicoherence of the 220ms slice, in which the frequency space has been restricted to remove duplicate information. For both simulated and measured data five wave ensemble averages have been performed, and the time window of the spectrogram selected to be 1.024 ms. Two f_l bands can be identified: $0 < f_l < 60$ kHz and $200 < f_l < 300$ kHz. The low frequency peaks up to $f_l = 60$kHz are modulation

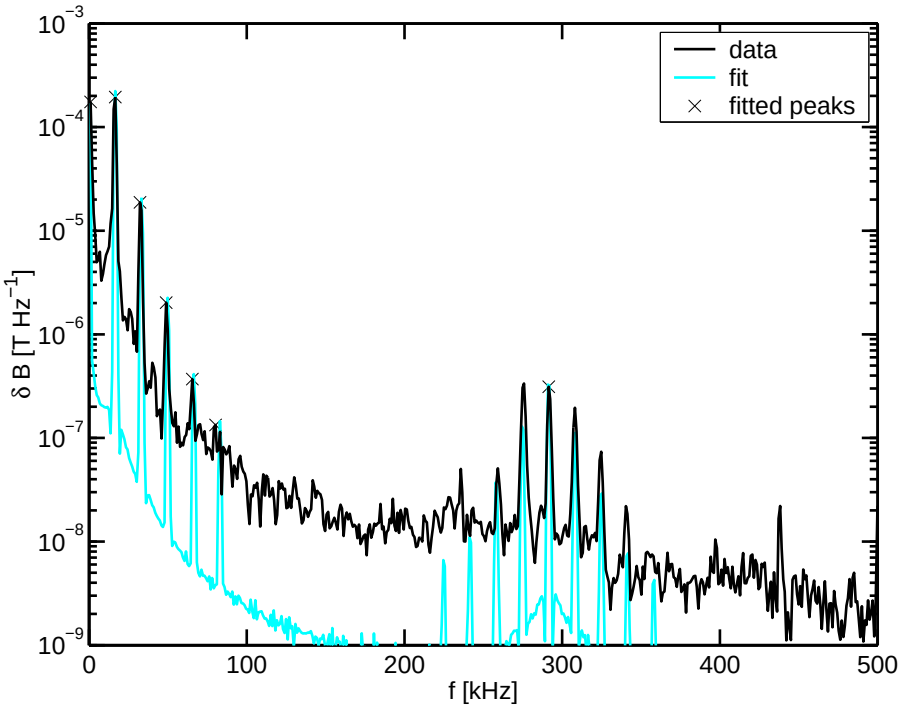

Figure 7. Spectrum of #9429 at 220ms, with predictions of the nonlinear model overlaid. The model comprises $n = 1$ 16kHz and $n = 8$ 290kHz driven frequency components, with the nonlinear model fitted to the low frequency modes envelope. The frequency, mode number of the tearing modes is a prediction of the nonlinear model, as is the frequency, mode number and side-band amplitude of the CAE $n = 8$ activity. Gaussian noise has been added to the fitted signal, with $\sigma = 0.001$ V. The cross-hairs denote observed peaks whose amplitude has been fitted.

of the low frequency modes. For example, the peak at $(f_l, f_k) = (16, 16)$ kHz is the interaction of the fundamental with the first harmonic at 32kHz, while the peak at $(f_l, f_k) = (16, 32)$ kHz is the interaction of the fundamental, first and second harmonics. The upper band at $200 < f_l < 300$ kHz is the interaction of low and high frequency modes.

A signal such as this, comprising the sum of two sinusoids driven nonlinearly to fifth order, will comprise 30 frequency components. Of these, 14 will have frequency below 200 kHz, yielding the 36 peaks in Fig. 8(b). For a coherent signal such as that considered here, peaks in the bicoherence are analogous to the quantified agreement in simulated frequency (identified by the spectrum of Fig. 7), and demonstrate frequency coupling between signal Fourier components.

The biphase reveals information about phase coupling. Figure 9 is a plot of measured biphase at peaks of the bicoherence along chords of constant ω_l, which have been marked accordingly in Fig. 8(b). In the simulated nonlinear model, the biphase is zero at all peaks of the bicoherence.

For the measurements, care has been taken to account for the inductor behaviour of the Mirnov coils, and to correct for the effects of alias. Correcting for the inductor

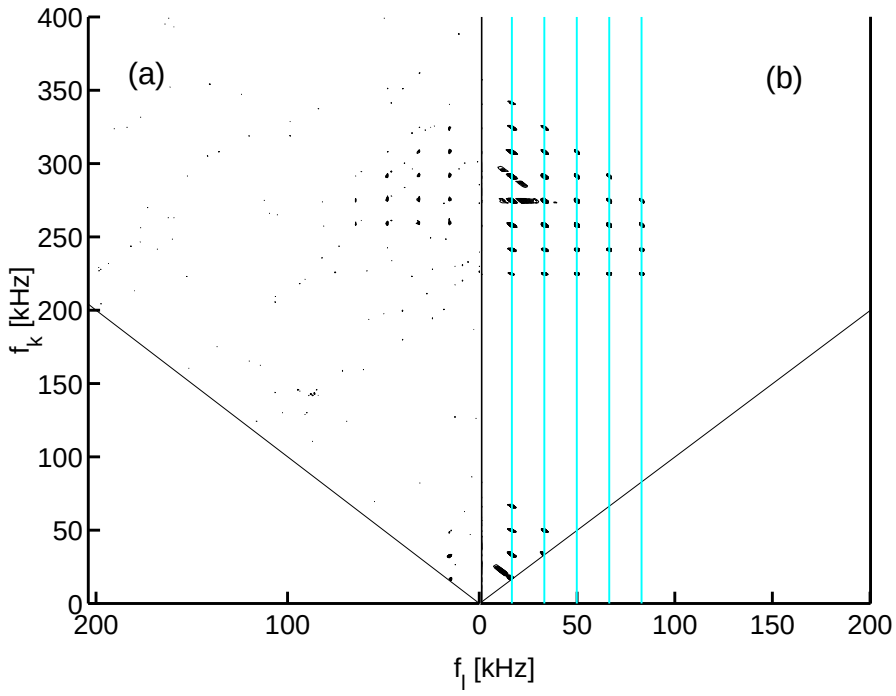

Figure 8. Bicoherence of #9429 at 220ms for (a) measured data and (b) nonlinear simulated fit. To aid resolution, only bicoherence values above a threshold $b_c > 0.9$ have been plotted, and the grayscale map has been chosen to highlight features. In (b), the light solid lines are chords of constant f_l.

behaviour involves ensuring a phase shift of $-\pi/2$ was applied to the computed Fourier transform of the data [cf. Eq. (1)]. Accounting for the effect of alias involves mapping the Fourier transform of the resulting signal $X(\omega)$ by

$$X(\omega_k)' = X(\omega_k), \qquad \omega < \omega_{low}, \omega_{high} < \omega \tag{12}$$

$$X(\omega_s - \omega_k)' = X(\omega_k)^*, \qquad \omega_{low} < \omega < \omega_{high} \tag{13}$$

where $\omega_s = 2\pi f_s$ is the angular sampling frequency, and $\omega_{low}, \omega_{high}$ the angular frequency interval over which the signal is aliased. The operation produces a Fourier transform splintered into the intervals $0 < \omega < \omega_{low}$, $\omega_{high} < \omega < \omega_s/2$ and $\omega_s - \omega_{low} < \omega < \omega_s + \omega_{high}$. For numeric convenience, we have eliminated frequency splintering by downshifting the sampling frequency in the mapping operation of Eq. (13) to $\omega_s = (\omega_{low} + \omega_{high})/2$.

At tearing mode modulation frequencies $f_l = 16, 32, 48, 80$ kHz the biphase is near zero, suggesting that the tearing modes are both phase-coupled and frequency-coupled, and so consistent with nonlinearly driven harmonics. In the alias shifted CAE mode frequency band, $100 < f < 400$ kHz, the biphase is nonzero. Further detail of the phase variation is provided by Fig. 10, in which the phase variation of the five chords has been unwrapped. Were the CAE modes phase uncoupled, the biphase at different frequencies

along each chord would be random. Instead, the variation of biphase with frequency along chords at 16 kHz and 32 kHZ is quadratic. In itself, this constitutes weak evidence of phase coupling.

We stengthen our phase-coupling claim by showing that such a quadratic frequency response could be generated if the CAE modes were phase-coupled to the tearing modes, and the transfer function for the phase of the complete system featured a cubic nonlinearity across the CAE frequency band. Our approach yields a self-consistent description of the data. The proof proceeds as follows.

Let the measured phase of the Fourier transform at frequency ω data be written as

$$\Phi(\omega) = \phi(\omega) + g(\omega) \tag{14}$$

with $g(\omega) = \angle H(\omega)$ the phase response of the system [cf. Eq. (1)]. At low frequency, $f < 100$ kHz, the tearing modes are phase-coupled, and the response of the system linear. The function $g(\omega)$ can be written

$$g(\omega) = \begin{cases} \alpha\omega & \omega < \omega_{linear} \\ \overline{g}(\omega) & \omega > \omega_{linear} \end{cases} \tag{15}$$

If $f_1 = \omega_1/(2\pi) < 100$ kHz and ω_2 is in the CAE angular frequency band, then the biphase can then be written

$$\angle B(\omega_1, \omega_2) = \Phi(\omega_1) + \Phi(\omega_2) - \Phi(\omega_1 + \omega_2) \tag{16}$$

$$= \phi(\omega_1) + \phi(\omega_2) - \phi(\omega_1 + \omega_2) + \alpha\omega_1 + \overline{g}(\omega_2) - \overline{g}(\omega_1 + \omega_2) \tag{17}$$

Our ansatz is that the signal is phase-coupled, and so $\phi(\omega_1) + \phi(\omega_2) - \phi(\omega_1 + \omega_2) = 0$. If we also suppose the phase response features a cubic nonlinearity, with

$$\overline{g}(\omega) = \beta_0 + \beta_1\omega + \beta_2\omega^2 + \beta_3\omega^3 \tag{18}$$

then

$$\angle B(\omega_1, \omega_2) = -3\beta_3\omega_1\omega_2^2 - (2\beta_3\omega_1^2 - 2\beta_2\omega_1)\omega_2 + (\alpha\omega_1 - \beta_1\omega_1 - \beta_2\omega_1^2 - \beta_3\omega_1^3) \tag{19}$$

We have fitted a quadratic polynomial to the phase variation over the first chord, and solved Eq. (19) for β_3, β_2 and $\alpha - \beta_1$. Using these polynomial coefficients, we have then computed the predicted phase variation for the next four chords. Agreement between the measured and predicted biphase is extremely good, with the error less than 15% over the range.

Figure 11 shows the computed phase profile response of the system. As described elsewhere [14], the system can be divided into three components: plasma-coil coupling, the coil-transmission line, and amplifier-digitiser. Each of these feature a phase response which monotonically decreases with increasing frequency. If each CAE sideband is resonant with an internal magnetic surface and q profile monotonic, then modes with increasing n (increasing frequency, decreasing aliased frequency) are localised closer to the core, and the coil-excitation-surface separation increases. In the absence of other plasma effects, the plasma-coil transfer function phase delay will increase with increasing n, and hence frequency. Providing that the coil-transmission line system has a real

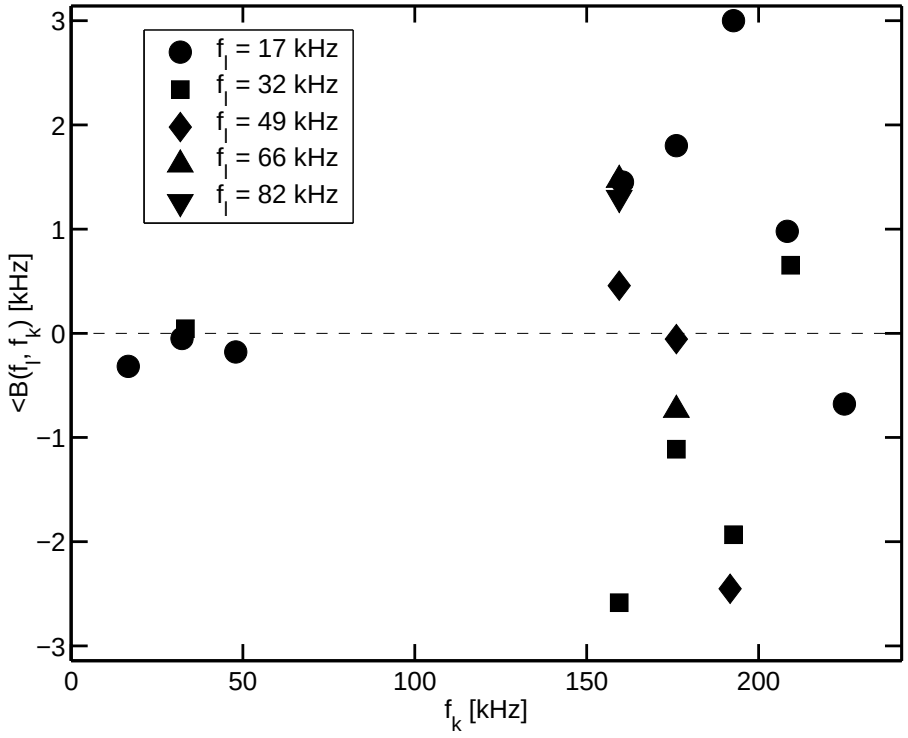

Figure 9. Biphase chords of #9429 at 220ms, taken at peaks in the bicoherence and for the chords identified in Fig.8. The different frequency chords are marked by different markers (see legend), and the dashed line of zero biphase is included for reference.

impedance termination (more precisely, the voltage reflection coefficient has magnitude below unity), which is true for the OMAHA coil set, the phase of the coil-transmission line transfer function will monotonically decreases with increasing frequency. As might be expected in an op-amp based amplifier, the higher frequencies are always phase delayed [27]. Qualitatively, the phase profile of Fig.11 is not inconsistent with the behaviour of the components.

Finally, we note that the toroidal mode number of each harmonic is consistent with modulation between an $n = 1$ and an $n = 8$ mode. That is, the tearing mode harmonics will have $n = 2, 3, 4, 5$, and the CAE sidebands will span $n = 10, 9, 8, 7, 6, 5$, which is observed.

5. Discussion

We have presented evidence of simultaneous high and low frequency magnetic activity in MAST, with near identical frequency splitting. The presence of low and high frequency components exists over a range of MHD modes, suggesting that the phenomena is not unique to a particular class of MHD activity. Motivated by such observations, we have postulated a modulation model, comprising the sum of two modes driven nonlinearly to large amplitude. The nonlinear order of the model is selected by the number of harmonics of the low frequency tearing mode activity, and the harmonic amplitudes

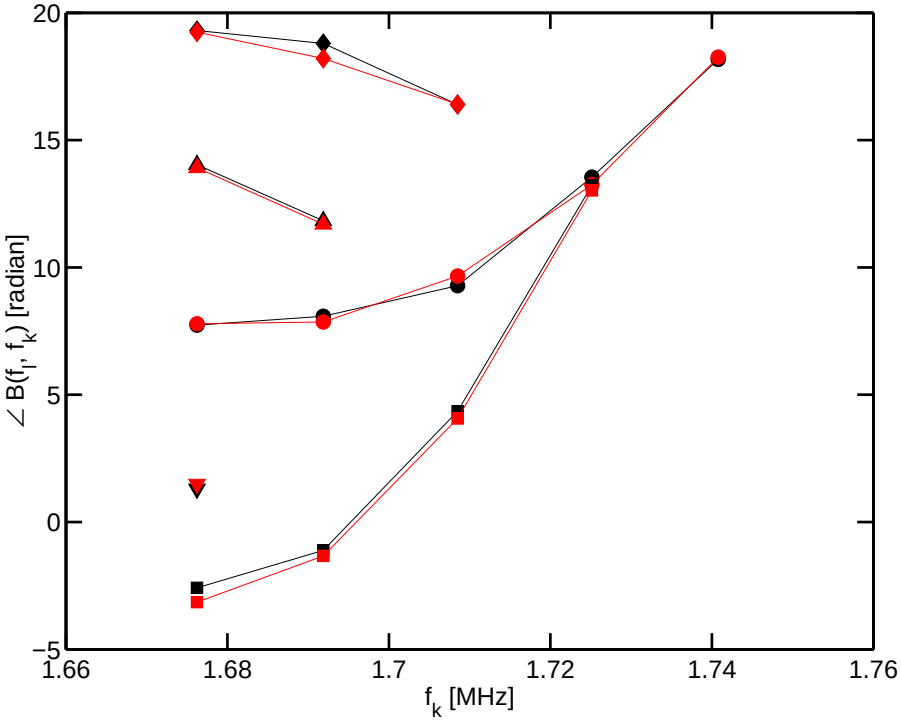

Figure 10. Unwrapped biphase chords of #9429 at 220ms over CAE frequency range, showing measured (black) and predicted (red) biphase. The same legend is used as in Fig.9.

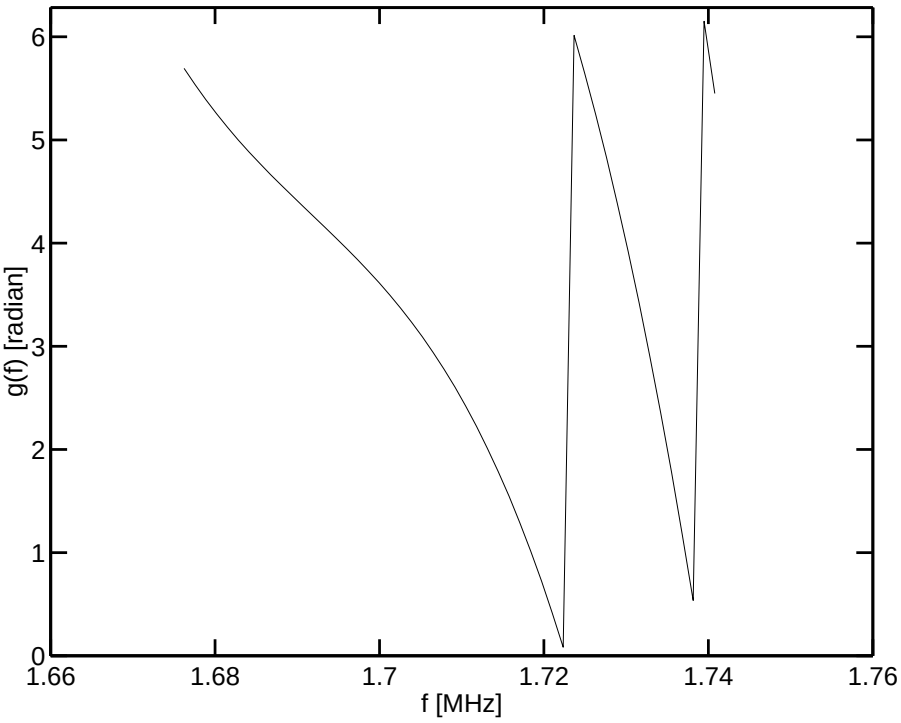

Figure 11. Modelled phase response of the amplifier, to within a linear frequency offset.

are used to fit for the model nonlinearity coefficients. The model has been applied to describe simultaneous low and high frequency activity in # 9429. For the low frequency components, the frequency spacing agrees extremely well with the measured data, and the phase difference between harmonics is near zero, in agreement with the nonlinear model. These conclusions are supported by bicoherence studies, which indicate frequency coupling, and an analysis of the biphase, showing phase coupling. The modulation of the low and high frequency components leads to sidebands of the CAE. Both the frequency spacing and amplitude profile of the sidebands are in good agreement with the nonlinear model. A study of the biphase indicates each frequency chord of the biphase has a quadratic dependence with frequency. These are found to be consistent with phase-coupling between CAE's and tearing modes, and a system response which features a cubic frequency dependence. The system frequency response exhibits increased phase delay with increasing frequency, and is qualitatively consistent with the product of plasma-coil, coil-transmission line, and amplifier-digitiser transfer functions, each of which feature a phase response which monotonically decreases with increasing frequency. Our self-consistent model for the biphase at CAE frequencies forms weak evidence for phase-coupling. In summary, we have provided evidence of frequency, mode number, and phase coupling between tearing modes and its harmonics and CAE's and its sidebands. Using a nonlinear modulation model, we have then shown amplitude-coupling between the CAE and it's sidebands. The nonlinear modulation model is also consistent with the observed frequency-coupling, mode number coupling, and low frequency phase-coupling.

Linear MHD theory computes the linear plasma response to a given Fourier perturbation. A theoretical treatment which predicts the nonlinear coefficients would require expansion of linear theory to the same nonlinear order as treated here. For a system with 5'th order nonlinearity, such an analysis is well beyond the scope of this work, even in simple geometry. Alternative approaches nevertheless exist that may shed light on the phenomena. For instance, MHD modulation models for mode coupling have been developed extensively in the space and solar physics literature. Karpman *et al* [28] have developed a reduced MHD nonlinear model to describe the modulational instability of whistler waves coupled to fast and slow magnetosonic waves. The main coupling between whistler and MHD waves is through the ponderomotive force, and so the coupling can be captured by the nonlinear Schrodinger equation. Fourier transformation leads to a Hamiltonian description, enabling long-time simulation of the modulational instability for the FMS- and SMS-whistler coupling in a 2D anisotropic slab geometry. Energy spreading to higher mode numbers behaves differently for the fast and slow modes, and the fast wave interaction leads to qausi-recurrent behaviour in whistler amplitude: the modulational instability is periodic. In comparison, long time simulation between the slow mode exhibits no such recurrent behaviour. The model is a paradigm for the modulational instability of waves in magnetized anisotropic plasmas.

An additional outcome of this work is clarification of the use and pitfalls of the bicoherence when trying to establish a phase-coupling conclusion. The bicoherence is

a good measure of phase-coupling only for signals which feature multiple mutually-incoherent wave bursts which each have a common power spectrum. In this instance, the averaging operation of the bispectrum becomes an ensemble average of wave packets with random initial phase. Only signals that are the product of nonlinear interaction will have the same phase relationship between components, and so sum to form a nonzero value of the bicoherence. Many plasma oscillations are however coherent, long-lived wave packets, and may evolve in frequency content between bursts. In these cases, the biphase at peak values in the bicoherence must also be investigated.

In future work, we intend to develop a similar simplified plasma model to Karpman *et al* , with the aim of qualitatively describing the phenomena discussed here, exploring the energy flow between modes, and possible consequent time evolution of the nonlinearity coefficients. In particular, we will try to establish whether a steady-state scenario exists, with time dependence that matches the observed signals. A second angle that will be explored is whether the sideband splitting and harmonics can be generated by computing the equilibrium and stability in 3D.

Acknowledgments

This work was partly funded by the Australian Research Council through grant DP0452728, the United Kingdom Engineering and Physical Sciences Research Council, and by the European Communities under the contract of Association between EURATOM and UKAEA. The views and opinions expressed herein do not necessarily reflect those of the European Commission.

References

[1] A. Fasoli, D. Borba, C. Gormezano, R. Heeter, A. Jaun, J. Jacquinot, W. Kerner, Q. King, J. B. Lister, S. Sharapov, D. Start, and L. Villard. Alfvén eigenmode experiments in tokamaks and stellarators. *Plas. Phys. Con. Fus.*, 39:B287–B301, 1997.

[2] A. Fasoli, B. N. Breizman, R. F. Heeter, M. S. Pekker, and S. E. Sharapov. Nonlinear splitting of fast particle driven waves in a plasma: observation and theory. *Phys. Rev. Lett.*, 81(25):5564–5567, 1998.

[3] H. L. Berk, B. N. Breizman, and M. Pekker. Nonlinear dynamics of a driven mode near marginal stability. *Phys. Rev. Lett.*, 1996.

[4] N. N. Gorelenkov, C. Z. Cheng, E. Fredrickson, E. Belova, D. Gates, S. Kaye, G. J. Kramer, R. Nazikian, and R. White. *Nucl. Fus.*, 42:977, 2002.

[5] N. N. Gorelenkov, E. D. Fredrickson, W. W. Heidbrink, N. A. Crocker, S. Kubota, and W. A. Peebles. Discrete compressional Alfvén eigenmode spectruum in tokamaks. *Nucl. Fusion*, 46:S933–S941, 2006.

[6] N. N. Gorelenkov and C. Z. Cheng. *Nuc. Fus.*, 35(12):1743–1752, 1995.

[7] N. N. Gorelenkov, C. Z. Cheng, and E. Fredrickson. *Phys. Plas.*, 9(8):3483–3488, 2002.

[8] H. Smith, T. Fulop, M. Lisak, and D. Anderson. Localisation of compressional Alfven eigenmodes in spherical torii. *Phys. Plas.*, 10(5):1437–1442, 2003.

[9] W. W. Heidbrink, E. D. Fredrickson, N. N. Gorelenkov, T. L. Rhodes, and M. A. Van Zeeland. Observation of compressional Alfvén eigenmodes (CAE) in a conventional tokamak. *Nuc. Fus.*, 46:324–334, 2006.

[10] L. C. Appel, T. Fulop, M. J. Hole, and H. M. Smith. Compressional Aflvén eigenmodes on MAST. *Plas. Phys. Con. Fus.*, submmitted.

[11] J. M. Mendel. Tutorial on Higher-Order Statistics (Spectra) in Signal Processing and System Theory: Theoretical Results and Some Applications. *Proc. IEEE*, 1991.

[12] J. W. A. Fackrell. *Bispectral Analysis of Speech Signals.* PhD thesis, University of Edinburgh, 1996.

[13] M. J. Hole and L. C. Appel. A novel technique for eigenmode analysis. In *Proc. 30th EPS Conf. Controlled Fusion Plas. Physics*, volume 27A, pages P–3.132, St Petersburg, Russia, July 2003.

[14] L. C. Appel and M. J. Hole. Calibration of the high-frequency magnetic fluctuation diagnostic in plasma devices. *Rev. Sci. Instrum.*, 76(9), Sep. 2005.

[15] M. J. Hole and L. C. Appel. Fourier decomposition of magnetic perturbations in toroidal plasmas using singular value decomposition. *Plas. Phys. Con. Fus.*, 49:1971–1988, 2007.

[16] R. J. Buttery *et. al.* Stability at High Performance in the MAST Spherical Tokamak. *Nuc. Fus.*, 44:1027–1035, 2004.

[17] D. F. Howell, T. C. Hender, and G. Cunningham. Locked modes thresholds on the MAST spherical tokamak. *Nuc. Fus.*, 47:1336–1340, 2007.

[18] Y. C. Kim and E. J. Powers. Digital bispectrum analysis and its applications to nonlinear wave interactions. *IEEE Trans. Plas. Science*, PS-7(2):120–130, 1979.

[19] M. Abramowitz and I. A. Stegun. *Handbook of Mathematical Functions.* Dover, 1964.

[20] T. J. Maccarone and J. D. Schnittman. The bicoherence as a diagnostic for models of high-frequency quasi-periodic oscillations. *Mon. Not. R. Astron. Soc.*, 357(12-16), 2005.

[21] D. Raju, O. Sauter, and J. B. Lister. Study of nonlinear mode coupling during neoclassical tearing modes using bispectrum analysis. *Plas. Phys. Con. Fus.*, 45:369–378, 2003.

[22] K. Itoh, Y. Nagashima, S.-I. Itoh, P. H. Diamond, A. Fujisawa, and M. Yagi amd A. Fukuyama. On the bicoherence analysis of plasma turbulence. *Phys. Plas.*, 12:102301, 2005.

[23] A. E. White, S. J. Zweben, M. J. Burin, T. A. Carter, T. S. Hahm, J. A. Krommes, and R. J. Maqueda. Bispectral analysis of low- to high-confinement mode transitions in the National Sperical Tokamak Experiment. *Phys. Plas.*, 13:072301, 2006.

[24] D. R. Austin, M. J. Hole, P. A. Robinson, Iver H. Cairns, and R. S. Dallaqua. Laboratory Evidence for Stochastic Plasma-Wave Growth. *Phys. Rev. Lett.*, 99:205004, 2007.

[25] M. J. Hole, R. S. Dallaqua, S. W. Simpson, and E. Del Bosco. Plasma instability of a vacuum arc centrifuge. *Phys. Rev. E*, 65:046409, 2002.

[26] P. A. Robinson. *Phys. Plasmas*, 2:1466–1479, 1995.

[27] A. S. Sedra and K. C. Smith. *Microelectronic circuits.* Saunders College Publishing, 1991.

[28] V. I. Karpman, J. P. Lynov, P. K. Michelsen, and J. Juul Rasmussen. Nonlinear evolution of whistler wave modulational instability. *Phys. Plas.*, 2(9):3302–3319, 1995.